HHS Public Access

Author manuscript

Biochemistry. Author manuscript; available in PMC 2016 October 04.

Published in final edited form as:

Biochemistry. 2015 October 6; 54(39): 6123–6131. doi:10.1021/acs.biochem.5b00417.

Membrane interaction of the factor VIIIa discoidin domains in atomistic detail

Jesper J. Madsen[1,2], **Y. Zenmei Ohkubo**[3], **Günther H. Peters**[2], **Johan H. Faber**[4], **Emad Tajkhorshid**[3,5,*], and **Ole H. Olsen**[1,*]

[1] Haemophilia Biochemistry, Novo Nordisk A/S, DK-2760 Måløv, Denmark.

[2] Department of Chemistry, Technical University of Denmark, DK-2800 Kgs. Lyngby, Denmark.

[3] Beckman Institute for Advanced Science and Technology, University of Illinois at Urbana-Champaign, Urbana, Illinois 61801, USA.

[4] Protein Characterisation, Novo Nordisk A/S, DK-2760 Måløv, Denmark.

[5] Department of Biochemistry, College of Medicine, and Center for Biophysics and Computational Biology, University of Illinois at Urbana-Champaign, Urbana, Illinois 61801, USA.

Abstract

A recently developed membrane-mimetic model was applied to study membrane interaction and binding of the two anchoring C2-like discoidin domains of human coagulation factor (F)VIIIa, the C1 and C2 domains. Both individual domains, FVIII C1 and FVIII C2, were observed to bind the phospholipid membrane by partial or full insertion of their extruding loops (the spikes). However, the two domains adopted different molecular orientations in their membrane-bound states; FVIII C2 roughly positioned normal to the membrane plane, while FVIII C1 displayed a multitude of tilted orientations. The results indicate that FVIII C1 may be important in modulating the orientation of the FVIIIa molecule to optimize the interaction with FIXa, which is anchored to the membrane via its γ-carboxyglutamic acid-rich (Gla)-domain. Additionally, a structural change was observed in FVIII C1 in the coiled main chain leading the first spike. A tight interaction with one lipid per domain, similar to what has been suggested for the homologous FVa C2, is characterized. Finally, we rationalize known FVIII antibody epitopes and the scarcity of documented hemophilic missense mutations related to improper membrane binding of FVIIIa, based on the prevalent non-specificity of ionic interactions in the simulated membrane-bound states of FVIII C1 and FVIII C2.

[*]**Correspondence** Emad Tajkhorshid, Beckman Institute, 405 N Mathews Ave, Urbana, IL 61801, USA. Tel.: +1 217 244-6914. emad@life.illinois.edu, Ole H. Olsen, Novo Nordisk A/S, Novo Nordisk Park, F5.1.29, DK-2760 Måløv, Denmark. Tel.: +45 3075 4511. oho@novonordisk.com.

Author Contributions

J.J.M. designed the research, performed the research, analyzed data, and wrote the manuscript. Y.Z.O. designed the research, contributed analytic tools, analyzed data, and revised the manuscript. G.H.P. and J.H.F. designed the research, analyzed data, and revised the manuscript. E.T. and O.H.O. designed the research, analyzed data, provided computational resources, and revised the manuscript.

Keywords

Blood Clotting; Coagulation Factor VIII; fXase; Intrinsic Tenase; Membrane Proteins; Molecular Dynamics Simulations

The biochemical processes governing blood clotting are classically represented by a 'waterfall' or 'cascade' model [1,2]. Two distinct pathways (intrinsic *vs.* extrinsic) funnel into a common amplification phase where activated factor (F)X (FXa) is generated which, together with its cofactor FVa, is responsible for the burst of thrombin that subsequently leads to fibrin clot formation. The biomolecular components FVIII and FIX are circulating in the bloodstream as their inactive precursors, which upon activation assemble on a phospholipid surface into the highly potent FX-activating (FXase, also referred to as tenase) complex. Hemophilia A, the most common bleeding disorder by far [3], is characterized by deficiency in FVIII activity observed either as low levels, dysfunction of the protein procofactor, or the presence of inhibitory antibodies.

A pivotal aspect of the coagulation cascade is the ability of restricting blood clotting to the injury site. The platform for this spatial localization is provided by the activated platelet membrane surfaces, which attract and stimulate activity by means of both membrane composition and the presence of elevated levels of certain cofactors to the coagulation enzymes. The tenase components FIXa and FVIIIa have the ability to selectively recognize this platform. Once properly bound and the binary complex formed, the catalytic efficiency of FIXa is up-regulated by approximately five orders of magnitude [4]. Membrane binding modes of FVIIIa and FIXa, however, are quite different; FIXa is anchored to the membrane by its vitamin K-dependent γ-carboxyglutamic acid-rich (Gla)-domain, while the membrane-targeting modules of FVIIIa are the two C2-like discoidin domains, C1 and C2, which recognize phosphatidylserine (PS)-containing platelet or endothelial cell membranes in a Ca^{2+}-independent manner [5]. While either domain (FVIII C1 or FVIII C2) by itself appears to be able to recruit the entire cofactor molecule to phospholipid membranes [6–10], optimal biological activity most certainly requires both.

The active cofactor molecule, FVIIIa, consists of three polypeptide chains forming five major domains (A1, A2, and the light chain A3-C1-C2) with a total of more than 1,200 amino acid residues. The structural topology of the C1 and C2 domains is that of lectin and commonly known as a jelly-roll β-barrel (Fig. 1A); eight anti-parallel β-strands are arranged in two major β-sheets, wrapped to form the barrel and then flattened to a sandwich-like shape [11]. Connecting the β-strands at the bottom of the barrel are four hairpin loops also called the spikes (S1-S4, Fig 1A) or fatty feet [12], the latter designation being due to the presence of multiple solvent exposed hydrophobic residues. These spikes are of particular importance for platelet membrane-aided functionalities because S1-S4 are hypothesized to be inserted into the hydrophobic core of the phospholipid membrane [7,13]. For this reason, much attention has been dedicated in the literature (e.g. by alanine mutagenesis [14], motif mutagenesis [15] and loop-swaps [12]) to elucidate how affinity and specificity of the FVIIIa molecule (and FVIII C2 on its own) toward phospholipid membranes is controlled by the residues in these spikes. The primary membrane-anchoring domain of FVIIIa is

conventionally thought to be the C2 domain [16]. Recently, however, several studies have emphasized the important role of the C1 domain in the membrane-mediated cofactor function of FVIIIa [6,8,15,17–21].

Previous studies on the molecular orientation of FVIIIa suggest a crystal structure-like domain configuration with a membrane-bound configuration in which the molecule is close to perpendicular to the membrane plane (or slightly tilted) with both FVIII C1 and FVIII C2 peripherally inserted in the membrane [22–24]. A fundamentally different interaction, requiring large scale domain rearrangements to accommodate a binding mode where solely FVIII C2 interacts with the membrane and is deeply inserted, has been suggested based on cryo-electron microscopy experiments in conjugation with a membrane model consisting of lipids assembled on nanotubes [25–28]. In addition, concurrent domain conformational span between C1 and C2 has been reported for the homologous coagulation factor Va in a study utilizing atomic force microscopy [29].

The membrane interaction of FVIII C2-like domains has very recently been explored using molecular simulations at the coarse-grained level of theory [30]. While coarse-graining is appropriate for comparing membrane binding times between domains and mutants, unfortunately atomistic details possibly governing specific interactions with the membrane are not readily discernible. Therefore, we have conducted all-atom simulations to give a detailed characterization of the individual discoidin domains from human coagulation FVIIIa in the membrane-bound state with respect to lipid specificity, molecular orientation and flexibility. These are properties of fundamental importance for the cofactor activity of FVIIIa in the intrinsic tenase complex. The all-atom classical molecular dynamics (MD) simulation technique provides sufficiently high spatial and temporal resolutions to generate detailed information on the atomic level of the membrane binding and lipid interaction of the FVIIIa C2-like domains. In order to expedite the dynamics of membrane lipids and therefore accelerate the membrane binding of the C2-like domains, the use of the Highly Mobile Membrane Mimetic (HMMM) model [31] is adopted. This enables multiple occurrences of membrane binding (of C2-like domains) in relatively short, independent trajectories. Hence, an improved statistical representation of the dynamics becomes feasible.

The article is structured as follows. The protein-lipid interaction of each of the two membrane-anchoring discoidin domains from human FVIIIa (FVIII C2 and FVIII C1) is characterized, and a PS-binding motif is described. The achieved membrane-bound states are discussed in relation to haemophilic disease mutations, antibody binding epitopes, and a putative tenase complex model.

Materials and Methods

Model building and initial setup

The starting structures of FVIII C1 and FVIII C2 domains were taken from the crystallized B-domain-less human FVIII with PDB ID code 3cdz [22] (residues 2021-2172 for FVIII C1; residues 2173-2332 for FVIII C2). It can be safely assumed that there is little or no structural distinction between these domains in FVIII and FVIIIa, both in the context of the full-length (pro)cofactor and cut-out on their own. pKa calculations were performed using PROPKA [32]

to assign protonation states to titratable side chains consistent with pH 7; no deviation from standard titration states was necessary.

To assemble the HMMM membrane [31], short-tailed (st-)lipid molecules truncated at the C_5 carbon atom containing a PS headgroup (*i.e.* divalerylphosphatidylserine, DVPS; see Ohkubo *et al.*[31] for the details) were packed to sandwich a layer of 1,1-dichloroethane (DCLE) solvent molecules with the lipid headgroups facing the water phase and acyl chains against the DCLE organic phase using Packmol [33].

The individual FVIII C1 and FVIII C2 domains (Fig. 1A) were then manually placed above the membrane such that the β-barrel central axis (the third principal axis of inertia) was oriented approximately parallel to the membrane normal ($\theta =\sim 0$; Fig. 1B) with the hydrophobic membrane-anchoring spikes facing the membrane (Fig. 1B). The spikes are defined as follows. S1 is residues 2043-2046 for FVIII C1 and 2196-2203 for FVIII C2; S2 is residues 2056-2059 for FVIII C1 and 2213-2217 for FVIII C2; S3 is residues 2089-2096 for FVIII C1 and 2248-2255 for FVIII C2; S4 is residues 2156-2159 for FVIII C1 and 2313-2316 for FVIII C2. The resulting systems (denoted C2/HMMM and C1/HMMM) which contained an HMMM patch and a C2-like domain were solvated by water molecules and neutralized with sodium (Na^+) ions using the SOLVATE and AUTOIONIZE plugins of VMD [34]. Water molecules placed by SOLVATE within the DCLE organic solvent phase of the membrane (due to the presence of initially large gaps) were removed. A reference system was prepared in a similar fashion and contained only FVIII C2 in bulk water (C2/Soln) at physiological 150 mM NaCl. The details of the individual systems simulated are provided in Table 1.

Simulation details

The prepared systems (C2/HMMM and C1/HMMM) were initially energy-minimized by applying the conjugated gradient method for 5,000 steps. Then the systems were subjected to a short (100 ps) simulation in the *NPT* ensemble with constant aspect ratio of the membrane plane (x/y) to resolve imperfect packing of DCLE molecules, and hence equilibrate the membrane thickness. During this phase, the area per lipid in the systems was free to change and resulting values ranged from 85.0 Å to 88.5 Å (prior to protein insertion). While this is somewhat larger than the values for pure lipid bilayers [35,36], it is designed to take into account the approximate area that would be occupied by insertion of the protein domains. Once the membrane thickness was stable, a mild harmonic constraint with a small force constant of 0.01 kcal mol^{-1} $Å^{-2}$ along the z-axis was applied on the C_2 carbon atoms of all st-lipids to restrain them around the average height of all C_2 atoms in their respective membrane leaflet. This was done to gently reduce vertical diffusion (along the z-axis) of the st-lipids and to eliminate potential net translation of the system along the z-axis, as well as to discourage lipid inversion. Using the resulting system as an initial structure, the production MD simulations were performed 5 times independently for each system in the *NPnAT* ensemble with the target pressure and temperature of $P = 1$ atm and $T = 310$ K controlled by the Nosé-Hoover Langevin piston barostat [37,38] and the Langevin thermostat (damping coefficient: 5/ps) [39], respectively. The solution system (C2/Soln) was prepared in the same way, except no treatments for the non-present lipids. Throughout, pressure coupling was

applied along the membrane normal, *n* (piston damping coefficient: 5/ps, piston period: 100 fs), and piston decay: 50 fs).

Long-range electrostatic forces were calculated using the particle mesh Ewald (PME) method [40,41] with a grid spacing of approximately 1 Å and a fourth-order spline for interpolation. Electrostatic forces were updated every 4 fs. van der Waals interactions were cut off at 12 Å in combination with a switching function beginning at 10 Å. Periodic boundary conditions were applied in the *x*-, *y*-, and *z*-directions. All MD simulations were performed using NAMD 2.9 [42] with the CHARMM27 force field/CMAP correction [43,44] for proteins, CHARMM36 [45] for lipid topology, and the TIP3P model for water [46]. An integration time step of 2.0 fs was used for the velocity Verlet algorithm with SHAKE [47]. All analyses and visualization of molecular structures and trajectories were done using VMD 1.9.1 [34]; calculation of van der Waals and electrostatic interaction energies between the protein and the membrane was done using the NAMDENERGY plugin of VMD without PME. Plots were prepared using Grace (xmgrace, http://plasma-gate.weizmann.ac.il/Grace).

Calculation of order parameters for backbone ($C_i - N_i$) vectors

The backbone C-N vector was defined for each individual amino acid residue as the normalized vector pointing from the backbone carbonyl carbon atom to the backbone amide nitrogen atom. The protein was aligned over the trajectory by a root mean square deviation-based structural alignment on all heavy atoms. Following this, nematic order parameters were calculated as described in Cecchini *et al.*[48]

$$S_i^2 = \left\langle \frac{3}{2}\left(\hat{\mathbf{z}}_i \cdot \hat{\mathbf{d}}_i\right)^2 - \frac{1}{2} \right\rangle$$

where S_i^2 is the order parameter for the *i*th residue, $\hat{\mathbf{d}}_\mathbf{i}$ (the director) is a unit vector describing the trajectory-averaged vector from C_i to N_i in the residue *i* of the aligned trajectory, and $\hat{\boldsymbol{z}}_\mathbf{i}$ is the instantaneous atomic $C_i - N_i$ unit vector for residue *i*. The brackets denote averaging over the trajectory. The frame rate for the analysis was 10 frames per ns. The order parameters assume values from 0 to 1 and they are a measure of how much the atomic backbone vectors fluctuate around their respective trajectory-averaged directions, indicating the flexibility of the backbone at that given position in the structure.

Time-averaged analyses for the membrane-bound state

The domain tilt angles of FVIII C1 and FVIII C2, membrane-contacting frequencies for each amino acid residue, and backbone order parameters are calculated only for the part of the simulated trajectories where the domain is associated with the membrane based on a 5-Å proximity criterion.

Construction of a putative model of the FVIIIa:FIXa tenase complex

A putative model of the FVIIIa:FIXa tenase complex was constructed on the basis of the recently published X-ray crystallographic structure of the FVa:FXa prothrombinase complex from the venom of the eastern brown snake [49]. The light chain of FIXa in the constructed tenase complex was modeled in a FVIIa-like extended conformation [50], instead of an arched

conformation adopted by procine FIXa with a partially disordered Gla-domain (L chain of PDB ID code 1pfx [51]). Homologous molecules (FVa versus FVIIIa, and FIXa versus FXa) were aligned and the missing loops were constructed with the molecular modeling package Quanta (Molecular Simulations Inc., San Diego, CA). The atomic coordinates of the model are available upon request.

Results and Discussion

Membrane-binding simulations started with the anchoring domains initially placed over the membrane without any contacts. The positively charged FVIII C1 and FVIII C2 domains are attracted to the negatively charged phospholipid membrane due to favorable electrostatic interactions, shown by the calculated non-bonded interaction energies between the domain and the membrane (Fig. 2, *bottom*, and Fig. S1 in the Supporting Material). As we describe in the following, the five parallel FVIII C2 trajectories converged into a stable membrane-bound state with comparable spike insertion depths and domain tilt angles (Fig. 1C). Sequence identity shared by FVIII C1 and FVIII C2 is 40% and structural alignment of the two shows a sub-Ångström root mean square deviation of 0.90 Å based on the crystal structure [22]. The amino acid residues directly involved in membrane binding and their specific sequence of interaction varied depending on the orientation of the studied FVIIIa domain upon membrane contact.

In the membrane-bound state of FVIII C2, a snug PS interaction via either R2220 or R2320 (Fig. 3) was achieved. This configuration was not observed in any of the four membrane-binding trajectories of FVIII C1 (one trajectory did not result in spontaneous binding and was discarded from further analysis) which instead displayed a broad range of domain tilt angles and significant structural modulations. Furthermore, the characteristic tight PS interaction with the residue corresponding R2320 in FVIII C1, R2163, was only observed in one trajectory. For both FVIII C1 and FVIII C2, the observed tightly-bound lipid is further stabilized by polar interactions of the amino and phosphate groups with residues of the protein, but these depended on the lipid orientation at the PS specificity pocket [13]. These findings show that either domain can achieve a direct protein-lipid interaction where PS binds compactly. However, the observed propensities are surprising, considering experimental reports that show FVIII C2 binding to vesicles is not PS-specific [52].

FVIII C2 adopts a perpendicular membrane-bound configuration and achieves a direct PS interaction

The converged molecular orientation is characterized by the domain tilt angle (Fig. 1B), which exhibited only small angles with respect to the membrane normal (20-40 degrees; Fig. 4, *top*) and hence is consistent with the previously proposed perpendicular (or slightly tilted) mode of interaction [23] and also the respective entry in the OPM (Orientation of Proteins in Membranes) database [53] for FVIII (PDB ID code 2r7e [54]). Regions of FVIII C2 in contact with the membrane were largely confined to the spikes (Fig. 5, *top*). No significant structural modulations are observed for FVIII C2 upon membrane binding as indicated by the calculated backbone order parameters both for the membrane-bound simulations, C2/HMMM, (Fig. 5, *top*) and for FVIII C2 in bulk water, C2/Soln (Fig. S2), albeit a mild

overall stabilization can be detected for the membrane-bound form consistent with the conclusions of a recently published study of FVIII C2 by hydrogen-deuterium exchange mass spectrometry [9].

The extruding hydrophobic spikes (Fig. 1A) are inserted peripherally into the membrane as the relative height of the domain tends to decrease over time until convergence is achieved (Fig. 2, *left*). The membrane-contacting surface is confined to about one third of the whole domain that mostly includes S1-S4 (Fig. 1C). The basic residues of this region in FVIII C2 interact with the acidic PS lipids (either PO_4^- or COO^- functional group) in a mainly transient and non-specific way with two exceptions, R2220 and R2320. It is the unique combination of a soft funnel-like geometry of the loops in the membrane-interacting part of the domain and a centrally positioned arginine (either R2320 or R2220 depending on the domain tilt angle) that interacts selectively with the carboxylic acid group of the lipid that defines the direct interaction with PS (Fig. 3). This binding motif is further stabilized by polar interactions of the phosphate group of the lipid with surrounding amino acid residues of the protein.

It is interesting to note that while direct FVIII C2-PS interactions do occur, occasionally, via both R2320 and R2220, these residues seem to be mutually exclusive; in domain orientations that enable R2220 to be selectively engaged with the COO^- group of a PS lipid, R2320 cannot, and vice versa. Furthermore, the direct protein-PS interactions are observed less frequently than for FVa C2 studied previously [55]. In the present study, for FVIII C2, the direct lipid interactions of R2220 are found in two of the five trajectories (#3 and #4), where they exist in about ~80% of the simulation time in which the domain is membrane-bound. The R2320 interaction is found in two other C2/HMMM trajectories, #5 and #3, but only ~33% and ~10% of the membrane-bound simulation time, respectively.

A direct comparison with FVa C2 is complicated by subtle yet important differences in amino acid sequences and, in particular, by the fact that FVa C2 carries a higher net positive charge than FVIII C2, as conferred by a surplus of basic K and R residues over acidic D and E residues (+12 *e* for FV C2 and +6 *e* for FVIII C2). These differences have direct impact on membrane affinity and association kinetics [56]. While binding free energies can, in principle, be calculated from a sufficiently long equilibrium simulation where many binding/unbinding events occur, spontaneous membrane unbinding events have not been observed in this study, nor in other reported work to our knowledge.

FVIII C1 exhibits structural flexibility and has multimodal orientations in the membrane-bound state

While the profile of lipid interaction of FVIII C2 resembles that of FVa C2 [55], FVIII C1 is markedly different in two ways: the trajectories do not converge to a well-defined unimodal binding orientation (Fig. 4, *bottom*), and FVIII C1 in its membrane-bound form is characterized by shape modulations and disorder in the coiled main chain leading to Spike 1 (Fig. 5, *bottom*). There are two major contributions to the retardation of the binding motif that allow the FVIII C1 domain to adopt a variety of moderately to highly tilted molecular orientations in its membrane-bound form: 1) the loss of local structural integrity (Fig. S3) and 2) the fact that Spike 1 in FVIII C1 is four residues shorter than in FVIII C2, making it

extrude significantly less (Fig. 1A). The domain tilt angle is in general larger (relative to the membrane normal) for FVIII C1 than for FVIII C2; the averages of the angles for 4 individual C1/HMMM trajectories range between 30 and 65 degrees (Fig. 4, *bottom*).

The observed structural changes in FVIII C1 is facilitated by the breaking of the main chain H-bonds between Q2036 and K2072, which in the X-ray crystallographic structure clamp the surrounding loop region to the body of the domain (Fig. S3). Upon release, the main chain of the region centered around residue 2030 adheres to the membrane bilayer (Fig. 5, *bottom*) and interacts favorably with it, but in a non-specific manner. Such a structural mechanism or conformational change could explain, in part, why a complex multiphase binding mechanism is observed for FVIII [57]. The general trend of the calculated backbone order parameters clearly shows that FVIII C1 is more flexible than FVIII C2 (Fig. 5), in particular in those regions that are in contact with the membrane (including the spikes, and the loop region leading to Spike 1). Surprisingly, the C1 domain also exhibits increased flexibility in a loop, which is never observed to interact with the membrane (residues 2115-2123). The fact that FVIII C1 is relatively disordered (for such a β-rich domain) could further be involved in causing the scarcity of FVIII C1 domain structures available in the Protein Data Bank (PDB) [58]. There is supporting experimental evidence that those protein segments of FVIII C1 involved in the above described structural changes are indeed very flexible, as reflected in their high crystallographic temperature factors (PDB ID codes 3cdz [22] and 4bdv [59]).

A search for direct interactions between PS lipids and FVIII C1 (Fig. S4, *left*) reveals that around the key positions in FVIII C1, R2163 (the counterpart to R2320 in C2; Fig. 3) is the only residue observed to interact with the carboxylic acid group of the lipids, and only in a single trajectory. R2220 in FVIII C2 has no counterpart in FVIII C1; K2065 is the closest basic residue to this position according to structural alignment of the two domains, and this residue is positioned two residues downstream and interacts only non-specifically with either of the negatively charged functional groups of the lipids (PO_4^- or COO^-).

Dynamical interpretation of hemophilic missense mutations and antibody epitopes related to membrane-binding

Our results offer a dynamical interpretation of the available hemophilia A disease genotypes related to dysfunctional membrane association and binding of FVIIIa via its dual discoidin domains (described in the previous section), a novel approach made possible by the use of the HMMM. Previous analyses have inferred on the functional-structural causation of hemophilic missense mutations based upon either homology models [60,61] and/or X-ray crystallographic structures [62], both of which offer only static representations of the protein structure in the absence of a membrane. Mutations of special interest are those positioned at the membrane interacting surface of the C2-like domains and include the following basic residues: R2052, R2090, R2159, and R2163 in FVIII C1, and R2320 in FVIII C2. Caution must be taken when interpreting mutations. Potential pitfalls include not only usual statistical fallacies but also unknown interactions with other biochemical components. With these precautions in mind, we here adopt the palatable concept that a hemophilic disease

missense mutation located at the membrane-interacting surface patches of FVIII C1 or FVIII C2 is potentially caused by improper membrane binding.

As has been noted previously [62], it is remarkable that only few of the documented hemophilic missense mutations are positioned in the membrane-interacting patch (including the spikes) of the discoidin domains of FVIII (Fig. 5). Specifically, only two mutants (V2223M, positioned in between Spikes 2 and 3, and A2201P located in Spike 1) were proposed to disrupt membrane binding. This could suggest that the major components necessary for sufficient membrane interaction for FVIIIa *in vivo* are non-specific contributions, such as hydrophobic partitioning and electrostatics, consistent with the results of the simulations described here. Furthermore, alanine-scanning the FVIII C2 domain within a complete B-domainless FVIII molecule has suggested that primarily resides in structural regions of the domain (β-sheet forming residues) are functionally sensitive to mutation [63]. In addition to these general observations, our results further implicate R2163 in FVIII C1, and R2220 and R2320 in FVIII C2 as potentially critical residues in that they are the only basic residues capable of forming direct interactions with PS lipids. Notably, R2163 and R2320 are known to give rise to hemophilic conditions upon mutation (The Haemophilia A Mutation, Structure, Test and Resource Site; http://hadb.org.uk/).

Antibodies KM33 and ESH-4 are known to modulate FVIII cellular uptake and binding [18,19,64,65]. KM33 abrogates the interaction between FVIII and phospholipids by binding to regions 2092-2093 within S3 of FVIII C1 and 2158-2159 within S4 of FVIII C1 [20]. Analogously, ESH-4 binding epitopes have been narrowed down to regions 2192-2196 (N-terminal side of S1 of FVIII C2), 2210-2125 (containing S2 of FVIII C2), and 2313-2316 (S4 of FVIII C2) [66]. A third FVIII antibody, ESH-8, which does not interfere with phospholipid binding, binds to residues 2234-2238 in between S2 and S3 of FVIII C2, and to residues 2267-2270 in between S3 and S4 of FVIII C2. Our results show excellent agreement with the binding epitopes of antibodies KM33, ESH-4, and ESH-8, in that the first two have epitopes located entirely within the membrane-contacting interface of C1 or C2, while the last one binds solely to regions not in contact with the membrane (Fig. 5).

Proposed mechanism of membrane interaction for the full-length FVIII and implications for a putative FVIIIa:FIXa tenase complex

Based on our results for the membrane-bound states of FVIII C1 and FVIII C2, putative membrane-bound configurations of the intrinsic tenase complex are proposed. Overlaying the putative model of the FVIIIa:FIXa tenase complex (Fig. 6A) with the converged final membrane-bound orientations of the C2/HMMM simulations (Fig. 6B, *top*) we find that, in all cases, preferential positioning of the C2 domain gives rise to tenase complex models without any clashes with the membrane. However, the N-terminally positioned Gla-domain of FIXa at (around) its ω-loop is not in contact with the membrane, nor is the C1 domain of FVIII. There are structural models describing the interaction between membranes and the Gla-domains from, e.g., prothrombin [67] and FVIIa [68], which, due to the high degree of homology among Gla-domains, is expected to be very similar to the binding mode of the FIXa Gla-domain to membranes. On the contrary, when FVIII is overlaid with the final FVIII C1 domain orientations from the C1/HMMM simulations (Fig. 6B, *bottom*), two of

the resulting orientations cause significant clashes between the FVIII C2 domain and the membrane (trajectories #3 and #5). Trajectories #2 and #4 of the C1/HMMM simulations correspond to reasonable binding modes between the membrane and the tenase complex in which FVIII C1, FVIII C2 and FIXa Gla-domains are all anchored in the membrane. #2 looks intuitive where the entire complex is positioned normal to the membrane plane, while #4 is very similar to highly tilted orientation suggested by FRET measurements[24]. To capture the motional span and membrane-contact of the anchoring FVIII C1, FVIII C2, and FIX Gla of the putative tenase complex when overlaid with the performed membrane-binding simulations, said tenase complex (Fig. 6A) was structurally aligned to membrane-bound FVIII C2 (resulting from C2/HMMM simulations #1-#5) or to membrane-bound FVIII C1 (for C1/HMMM simulations #2-#5) in each simulation frame. The relative heights, *z*, of the FIX Gla ω-loop as well as Spike 1 from the neighboring C domain reveal that realistic binding modes for the tenase complex are achieved only for the C1/HMMM simulations, primarily trajectory #2, but also transiently for trajectories #4 and #5 (Fig. 7).

Collectively, these considerations indicate that optimal interaction between FVIII C2 and the membrane can be achieved without major domain rearrangements in FVIIIa, whereas FVIII C1 membrane interactions might induce domain rearrangements in FVIIIa. Bearing in mind the convergent nature of the FVIII C2 membrane-interaction (described above) and the fact that the only non-binding simulated system was C1/HMMM #1, we speculate that membrane association of FVIIIa is initiated by the FVIII C2 domain and that FVIII C1 facilitates further membrane-anchoring while reorienting the cofactor. In any case, our simulations clearly indicate that FVIII C1 plays an important role in modulating the orientation of the FVIII molecule for optimal interaction with FIXa in the membrane-bound state. Since it is known that FVIII binding to membranes involves a complex mechanism [57], and considering the coiled nature of the four-residue FVIII C1-C2 inter-domain linker (residues 2170-2173), domain rearrangements are plausible. The inter-domain flexibility of the full-length FVIIIa is unknown, in particular, whether and how the membrane selects for or induces certain relative domain configurations. Furthermore, there appear to be non-trivial differences in PS-specificity for membrane binding of FVIII and FVIIIa [69]. However, preliminary results of simulations of the crystal structure FVIII light chain bound to HMMM suggest that only minor relative domain rearrangements occur, supporting the validity of the presented rigid-body putative tenase complex model (data not shown). These concepts are intriguing and subject for further studies.

Conclusion

Through the application of a novel membrane model with enhanced lipid dynamics, we have been able to describe spontaneous membrane binding and insertion of two membrane-anchoring domains of human FVIII. The simulations show that peripheral binding of FVIII C1 and FVIII C2 domains is facilitated by insertion of the domain-extruding spikes into the membrane. For FVIII C2, the resulting domain orientations converge to be nearly membrane-perpendicular, while FVIII C1 undergoes a structural change and is orientationally promiscuous (it can adopt several tilted orientations in the membrane-bound state). For both discoidin C2-like domains of FVIIIa, the mode of interaction with the phospholipid membrane is characterized by initial non-specific attractive electrostatic

interactions and hydrophobic partitioning. The insertion of the membrane-anchoring domain spikes is followed by the maturation of direct and specific interaction with a lipid molecule that enters the PS pocket. This specific lipid-protein interaction is observed more frequently and consistently for FVIII C2 than for FVIII C1. Deep embedding of large parts of either discoidin C2-like domain, as has been suggested for FVIII C2 based on cryo-electron microscopy, is not observed.

Supplementary Material

Refer to Web version on PubMed Central for supplementary material.

Acknowledgements

J.J.M. is supported by a grant from Forsknings- og Innovationsstyrelsen (Danish Agency for Science, Technology and Innovation) and the Novo Nordisk R&D Science, Talent, Attraction and Recruitment (STAR) programme.

References

1. MacFarlane R. An enzyme cascade in the blood clotting mechanism, and its function as a biochemical amplifier. Nature. 1964; 202:498–499. [PubMed: 14167839]
2. Davie EW, Ratnoff OD. Waterfall Sequence for Intrinsic Blood Clotting. Science. 1964; 145:1310–1312. [PubMed: 14173416]
3. Marder VJ, Aird WC, Bennett JS, Schulman S, White GC. Hemostasis and Thrombosis: Basic Principles and Clinical Practice Sixth edit. LWW. 2012
4. Dieijen G, Van, Tans G, Rosing J, Hemker HC. The Role of Phospholipid and Factor VIIIa in the Activation of Bovine Factor X. J. Biol. Chem. 1981; 256:3433–3442. [PubMed: 6782101]
5. Lemmon MA. Membrane recognition by phospholipid-binding domains. Nat. Rev. Mol. Cell Biol. 2008; 9:99–111. [PubMed: 18216767]
6. Wakabayashi H, Griffiths AE, Fay PJ. Factor VIII lacking the C2 domain retains cofactor activity in vitro. J. Biol. Chem. 2010; 285:25176–84. [PubMed: 20529839]
7. Pratt KP, Shen BW, Takeshima K, Davie EW, Fujikawa K, Stoddard BL. Structure of the C2 domain of human factor VIII at 1.5Å resolution. Nature. 1999; 402:439–442. [PubMed: 10586887]
8. Hsu T-C, Pratt KP, Thompson AR. The factor VIII C1 domain contributes to platelet binding. Blood. 2008; 111:200–8. [PubMed: 17916745]
9. Pantazatos D, Gessner CR, Woods VL Jr, Gilbert GE. Changes in the Factor VIII C2 Domain upon Membrane Binding Determined by Deuterium Exchange Mass Spectroscopy. Biochem. J. 2014; 461:443–451. [PubMed: 24814520]
10. Gilbert GE. Factor VIII inhibitor epitopes and an enigma. Blood. 2013; 122:4160–4161. [PubMed: 24357711]
11. Sharon, N.; Lis, H. LECTINS. 2nd ed.. Springer; 2003.
12. Mertens K, Meijer AB. Factors VIII and V swap fatty feet. Blood. 2012; 120:1761–3. [PubMed: 22936738]
13. Macedo-Ribeiro S, Bode W, Huber R, Quinn-Allen MA, Kim SW, Ortel TL, Bourenkov GP, Bartunik HD, Stubbs MT, Kane WH, Fuentes-Prior P. Crystal structures of the membrane-binding C2 domain of human coagulation factor V. Nature. 1999; 402:434–9. [PubMed: 10586886]
14. Gilbert GE, Kaufman RJ, Arena AA, Miao H, Pipe SW. Four hydrophobic amino acids of the factor VIII C2 domain are constituents of both the membrane-binding and von Willebrand factor-binding motifs. J. Biol. Chem. 2002; 277:6374–81. [PubMed: 11698391]
15. Gilbert GE, Novakovic VA, Kaufman RJ, Miao H, Pipe SW. Conservative mutations in the C2 domains of factor VIII and factor V alter phospholipid binding and cofactor activity. Blood. 2012; 120:1923–32. [PubMed: 22613792]

16. Foster PA, Fulcher CA, Houghten RA, Zimmerman TS. Synthetic factor VIII peptides with amino acid sequences contained within the C2 domain of factor VIII inhibit factor VIII binding to phosphatidylserine. Blood. 1990; 75:1999–2004. [PubMed: 2110840]
17. Lü J, Pipe SW, Miao H, Jacquemin M, Gilbert GE. A membrane-interactive surface on the factor VIII C1 domain cooperates with the C2 domain for cofactor function. Blood. 2011; 117:3181–9. [PubMed: 21156843]
18. Meems H, Meijer AB, Cullinan DB, Mertens K, Gilbert GE. Factor VIII C1 domain residues Lys 2092 and Phe 2093 contribute to membrane binding and cofactor activity. Blood. 2009; 114:3938–46. [PubMed: 19687511]
19. Meems H, van den Biggelaar M, Rondaij M, van der Zwaan C, Mertens K, Meijer AB. C1 domain residues Lys 2092 and Phe 2093 are of major importance for the endocytic uptake of coagulation factor VIII. Int. J. Biochem. Cell Biol. 2011; 43:1114–21. [PubMed: 21497669]
20. Bloem E, van den Biggelaar M, Wroblewska A, Voorberg J, Faber JH, Kjalke M, Stennicke HR, Mertens K, Meijer AB. Factor VIII C1 Domain Spikes 2092-2093 and 2158-2159 Comprise Regions That Modulate Cofactor Function and Cellular Uptake. J. Biol. Chem. 2013; 288:29670–9. [PubMed: 24009077]
21. Wakabayashi H, Fay PJ. Replacing the factor VIII C1 domain with a second C2 domain reduces factor VIII stability and affinity for factor IXa. J. Biol. Chem. 2013; 288:31289–97. [PubMed: 24030831]
22. Ngo JCK, Huang M, Roth DA, Furie BC, Furie B. Crystal structure of human factor VIII: implications for the formation of the factor IXa-factor VIIIa complex. Structure. 2008; 16:597–606. [PubMed: 18400180]
23. Liu Z, Lin L, Yuan C, Nicolaes GAF, Chen L, Meehan EJ, Furie B, Furie B, Huang M. Trp2313-His2315 of factor VIII C2 domain is involved in membrane binding: structure of a complex between the C2 domain and an inhibitor of membrane binding. J. Biol. Chem. 2010; 285:8824–9. [PubMed: 20089867]
24. Wakabayashi H, Fay PJ. Molecular orientation of Factor VIIIa on the phospholipid membrane surface determined by fluorescence resonance energy transfer. Biochem. J. 2013; 452:293–301. [PubMed: 23521092]
25. Parmenter CDJ, Cane MC, Zhang R, Stoilova-McPhie S. Cryo-electron microscopy of coagulation Factor VIII bound to lipid nanotubes. Biochem. Biophys. Res. Commun. 2008; 366:288–93. [PubMed: 18039465]
26. Stoilova-McPhie S, Parmenter CDJ, Segers K, Villoutreix BO, Nicolaes GAF. Defining the structure of membrane-bound human blood coagulation factor Va. J. Thromb. Haemost. 2008; 6:76–82. [PubMed: 17949476]
27. Stoilova-McPhie S, Lynch GC, Ludtke S, Pettitt BM. Domain organization of membrane-bound factor VIII. Biopolymers. 2013; 99:448–459. [PubMed: 23616213]
28. Miller J, Dalm D, Koyfman AY, Grushin K, Stoilova-McPhie S. Helical organization of blood coagulation factor VIII on lipid nanotubes. J. Vis. Exp. 2014; 88:e51254.
29. Chaves RC, Dahmane S, Odorico M, Nicolaes GAF, Pellequer JL. Factor Va alternative conformation reconstruction using atomic force microscopy. Thromb. Haemost. 2014; 112:1167–1173. [PubMed: 25185589]
30. Du J, Wichapong K, Hackeng TM, Nicolaes GAF. Molecular simulation studies of human coagulation factor VIII C domain-mediated membrane binding. Thromb. Haemost. 2015; 113:373–384. [PubMed: 25354705]
31. Ohkubo YZ, Pogorelov TV, Arcario MJ, Christensen GA, Tajkhorshid E. Accelerating membrane insertion of peripheral proteins with a novel membrane mimetic model. Biophys. J. 2012; 102:2130–9. [PubMed: 22824277]
32. Li H, Robertson AD, Jensen JH. Very fast empirical prediction and rationalization of protein pKa values. Proteins. 2005; 61:704–21. [PubMed: 16231289]
33. Martínez L, Andrade R, Birgin EG, Martínez JM. Packmol : A Package for Building Initial Configurations. J. Comput. Chem. 2009; 30:2157–2164. [PubMed: 19229944]
34. Humphrey W, Dalke A, Schulten K. VMD: visual molecular dynamics. J. Mol. Graph. 1996; 14:33–38. [PubMed: 8744570]

35. Nagle JF, Tristram-Nagle S. Structure of lipid bilayers. Biochim. Biophys. Acta - Rev. Biomembr. 2000; 1469:159–195.
36. Petrache HI, Tristram-Nagle S, Gawrisch K, Harries D, Parsegian VA, Nagle JF. Structure and fluctuations of charged phosphatidylserine bilayers in the absence of salt. Biophys. J. 2004; 86:1574–86. [PubMed: 14990484]
37. Martyna GJ, Tobias DJ, Klein ML. Constant pressure molecular dynamics algorithms. J. Chem. Phys. 1994; 101:4177–4189.
38. Feller SE, Zhang YH, Pastor RW, Brooks BR. Constant pressure molecular dynamics simulation: The Langevin piston method. J. Chem. Phys. 1995; 103:4613–4621.
39. Allen, MP.; Tildesley, DJ. Computer simulation of liquids Reprint ed. Oxford University Press; 1989.
40. Darden T, York D, Pedersen L. Particle mesh Ewald: An N*log(N) method for Ewald sums in large systems. J. Chem. Phys. 1993; 98:10089–10092.
41. Essmann U, Perera L, Berkowitz ML, Darden T, Lee H, Pedersen LG. A smooth particle mesh Ewald method. J. Chem. Phys. 1995; 103:8577–8592.
42. Phillips JC, Braun R, Wang W, Gumbart J, Tajkhorshid E, Villa E, Chipot C, Skeel RD, Kalé L, Schulten K. Scalable molecular dynamics with NAMD. J. Comput. Chem. 2005; 26:1781–1802. [PubMed: 16222654]
43. MacKerell AD, Bashford D, Bellott M, Dunbrack RL, Evanseck JD, Field MJ, Fischer S, Gao J, Ha S, Joseph-McCarthy D, Kuchnir L, Kuczera K, Lau FTK, Mattos C, Michnick S, Ngo T, Nguyen DT, Prodhom B, Reiher WE, Roux B, Schlenkrich M, Smith JC, Stote R, Straub J, Watanabe M, Wiórkiewich-Kuczera J, Yin D, Karplus M. All-atom empirical potential for molecular modeling and dynamics studies of proteins. J. Phys. Chem. B. 1998; 102:3586–3616. [PubMed: 24889800]
44. MacKerell AD, Feig M, Brooks CL. Extending the treatment of backbone energetics in protein force fields: limitations of gas-phase quantum mechanics in reproducing protein conformational distributions in molecular dynamics simulations. J. Comput. Chem. 2004; 25:1400–15. [PubMed: 15185334]
45. Best RB, Zhu X, Shim J, Lopes PEM, Mittal J, Feig M, MacKerell AD. Optimization of the additive CHARMM all-atom protein force field targeting improved sampling of the backbone φ, ψ and side-chain χ(1) and χ(2) dihedral angles. J. Chem. Theory Comput. 2012; 8:3257–3273. [PubMed: 23341755]
46. Jorgensen WL, Chandrasekhar J, Madura JD, Impey RW, Klein ML. Comparison of simple potential functions for simulating liquid water. J. Chem. Phys. 1983; 79:926–935.
47. Ryckaert J, Ciccotti G, Berendsen H. Numerical integration of the cartesian equations of motion of a system with constraints: molecular dynamics of n-alkanes. J. Comput. Phys. 1977; 23:327–341.
48. Cecchini M, Rao F, Seeber M, Caflisch A. Replica exchange molecular dynamics simulations of amyloid peptide aggregation. J. Chem. Phys. 2004; 121:10748–56. [PubMed: 15549960]
49. Lechtenberg BC, Murray-Rust TA, Johnson DJ, Adams TE, Krishnaswamy S, Camire RM, Huntington JA. Crystal structure of the prothrombinase complex from the venom of Pseudonaja textilis. Blood. 2013; 122:2777–83. [PubMed: 23869089]
50. Banner DW, D'Arcy A, Chène C, Winkler FK, Guha A, Konigsberg WH, Nemerson Y, Kirchhofer D. The crystal structure of the complex of blood coagulation factor VIIa with soluble tissue factor. Nature. 1996; 380:41–46. [PubMed: 8598903]
51. Brandstetter H, Bauer M, Huber R, Lollar P, Bode W. X-ray structure of clotting factor IXa: active site and module structure related to Xase activity and hemophilia B. Proc. Natl. Acad. Sci. U. S. A. 1995; 92:9796–800. [PubMed: 7568220]
52. Novakovic VA, Cullinan DB, Wakabayashi H, Fay PJ, Baleja JD, Gilbert GE. Membrane-binding properties of the Factor VIII C2 domain. Biochem. J. 2011; 435:187–96. [PubMed: 21210768]
53. Lomize MA, Lomize AL, Pogozheva ID, Mosberg HI. OPM: orientations of proteins in membranes database. Bioinformatics. 2006; 22:623–5. [PubMed: 16397007]
54. Shen BW, Spiegel PC, Chang C-H, Huh J-W, Lee J-S, Kim J, Kim Y-H, Stoddard BL. The tertiary structure and domain organization of coagulation factor VIII. Blood. 2008; 111:1240–7. [PubMed: 17965321]

55. Ohkubo YZ, Tajkhorshid E. Exploring Membrane-Bound form of the C2 Domain by HMMM Model. Biophys. J. 2013; 104:432a. [PubMed: 23442865]
56. Mulgrew-Nesbitt A, Diraviyam K, Wang J, Singh S, Murray P, Li Z, Rogers L, Mirkovic N, Murray D. The role of electrostatics in protein-membrane interactions. Biochim. Biophys. Acta. 2006; 1761:812–26. [PubMed: 16928468]
57. Bardelle C, Furie B, Furie BC, Gilbert GE. Membrane binding kinetics of factor VIII indicate a complex binding process. J. Biol. Chem. 1993; 268:8815–24. [PubMed: 8473326]
58. Bernstein FC, Koetzle TF, Williams GJB, Meyer EF, Brice MD, Rodgers JR, Kennard O, Shimanouchi T, Tasumi M. The Protein Data Bank: a computer-based archival file for macromolecular structures. J. Mol. Biol. 1977; 112:535–542. [PubMed: 875032]
59. Svensson LA, Thim L, Olsen OH, Nicolaisen EM. Evaluation of the metal binding sites in a recombinant coagulation factor VIII identifies two sites with unique metal binding properties. Biol. Chem. 2013; 394:761–5. [PubMed: 23435097]
60. Pellequer JL, Gale AJ, Griffin JH, Getzoff ED. Homology models of the C domains of blood coagulation factors V and VIII: a proposed membrane binding mode for FV and FVIII C2 domains. Blood Cells. Mol. Dis. 1998; 24:448–61. [PubMed: 9880241]
61. Gale AJ, Pellequer JL, Getzoff ED, Griffin JH. Structural basis for hemophilia A caused by mutations in the C domains of blood coagulation factor VIII. Thromb. Haemost. 2000; 83:78–85. [PubMed: 10669159]
62. Liu ML, Shen BW, Nakaya S, Pratt KP, Fujikawa K, Davie EW, Stoddard BL, Thompson AR. Hemophilic factor VIII C1- and C2-domain missense mutations and their modeling to the 1.5-angstrom human C2-domain crystal structure. Blood. 2000; 96:979–87. [PubMed: 10910913]
63. Pellequer JL, Chen SW, Saboulard D, Delcourt M, Négrier C, Plantier JL. Functional mapping of factor VIII C2 domain. Thromb. Haemost. 2011; 106:121–131. [PubMed: 21614407]
64. Wroblewska A, van Haren SD, Herczenik E, Kaijen P, Ruminska A, Jin S-Y, Zheng XL, van den Biggelaar M, ten Brinke A, Meijer AB, Voorberg J. Modification of an exposed loop in the C1 domain reduces immune responses to factor VIII in hemophilia A mice. Blood. 2012; 119:5294–300. [PubMed: 22498747]
65. Brinkman H-JM, Mertens K, van Mourik JA. Phospholipid-Binding Domain of Factor VIII Is Involved in Endothelial Cell-Mediated Activation of Factor X by Factor IXa. Arterioscler. Thromb. Vasc. Biol. 2002; 22:511–516. [PubMed: 11884299]
66. Faber, JH.; Appa, RS.; Stennicke, H.; Kjalke, M. Contribution of C2 domain epitopes in FVIII cellular uptake assessed by epitope mapping of the anti-C2 antibodies ESH4 and ESH8 by hydrogen-deuterium exchange mass spectrometry. FASEB Summer Research Conference on Proteases in Hemostasis & Vascular Biology; Nassau, Bahamas. June 2–7; 2013.
67. Huang M, Rigby AC, Morelli X, Grant MA, Huang G, Furie B, Seaton B, Furie BC. Structural basis of membrane binding by Gla domains of vitamin K-dependent proteins. Nat. Struct. Biol. 2003; 10:751–6. [PubMed: 12923575]
68. Ohkubo YZ, Tajkhorshid E. Distinct structural and adhesive roles of Ca^{2+} in membrane binding of blood coagulation factors. Structure. 2008; 16:72–81. [PubMed: 18184585]
69. Engelke H, Lippok S, Dorn I, Netz RR, Rädler JO. FVIII binding to PS membranes differs in the activated and non-activated form and can be shielded by annexin A5. J. Phys. Chem. B. 2011; 115:12963–70. [PubMed: 21954889]

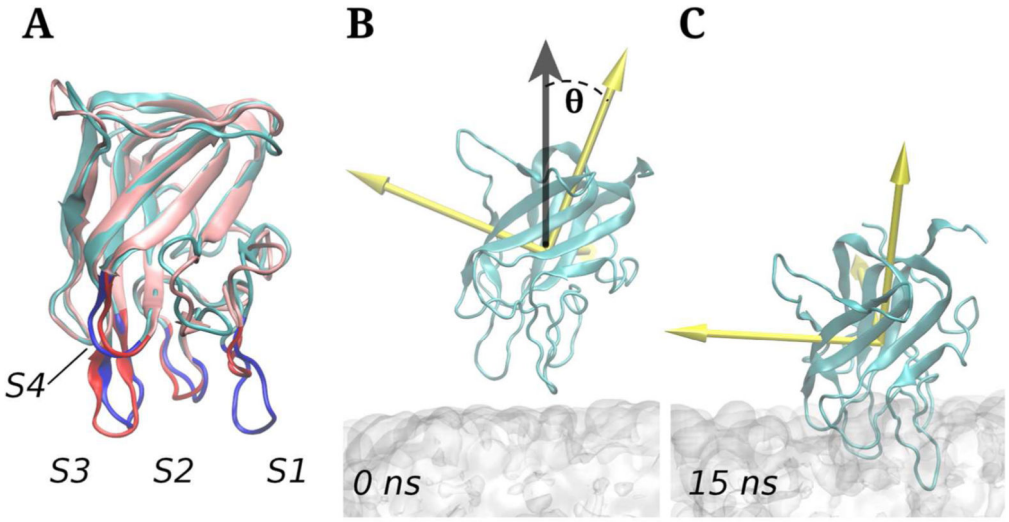

FIGURE 1.

(**A**) Structural alignment of FVIII C1 (pink) and FVIII C2 (cyan) based on PDB ID code 3cdz [22]. The spikes S1-S4 are highlighted in red for FVIII C1 and in blue for FVIII C2. (**B**) Representative domain orientation and position of the C2-like domain with respect to the surface of the membrane patch which was used in all the simulations as the starting configuration ($t = 0$). Depicted is FVIII C2 (in cartoon representation) and the HMMM patch (translucent gray). The yellow vectors show the principal axes of inertia of the FVIII C2 domain. The domain tilt angle, θ, is defined as the angle between the third principal axis of inertia and the membrane normal, z (gray vector). (**C**) Representative membrane-bound state of FVIII C2 with inserted spikes (snapshot taken at $t = 15$ ns from trajectory #2).

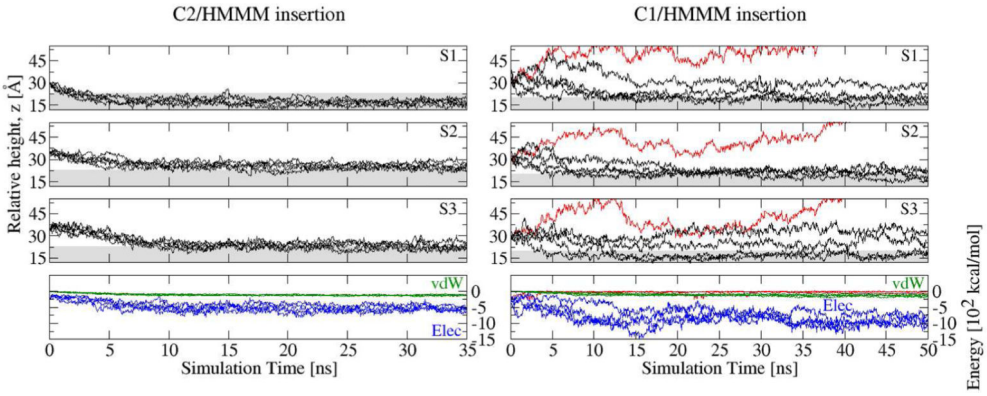

FIGURE 2.

(*Left*) Insertion depth of Spikes 1-3 (S1-S3) of FVIII C2 and interaction energy with the HMMM as functions of the simulation time for the five trajectories, #1-#5. Each spike depth is represented by a single α-carbon atom, namely G2044 for Spike 1, S2058 for Spike 2, and F2093 for Spike 3. (*Right*) Insertion depth of Spikes 1-3 of FVIII C1 and interaction energy with the HMMM as functions of the simulation time for the four binding trajectories, #2-#5, (black) and for the unproductive (non-binding) trajectory, #1 (red). Each spike depth is represented by a single α-carbon atom belonging to a representative residue, namely, M2199 for Spike 1, R2215 for Spike 2, and L2252 for Spike 3. In both panels, gray-shaded area represents the membrane region below the average plane of the phosphorus atoms (atom type P) of st-lipids. The membrane is centered at $z = 0$. Calculated non-bonded interaction energies (*bottom* panels) are broken into van der Waals (vdW, in green except for the unproductive simulation which is drawn in red) and electrostatic (Elec, in blue) components.

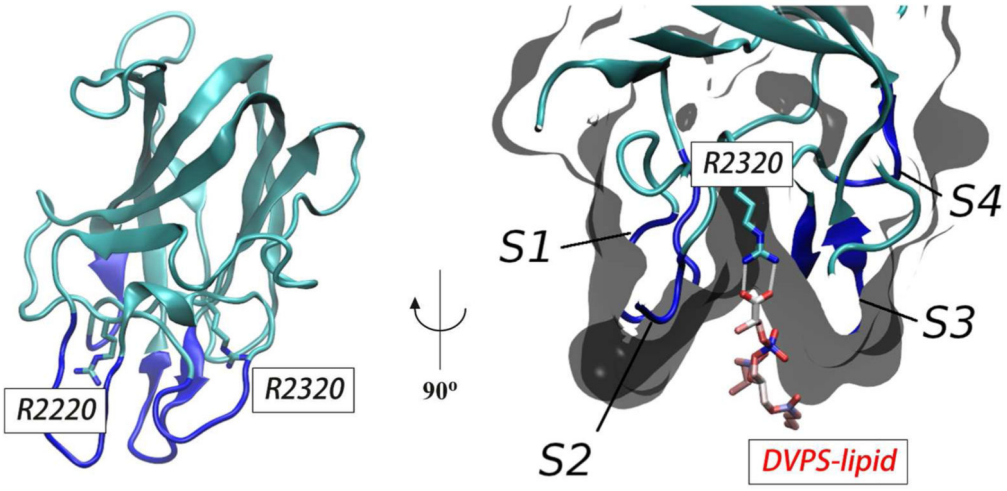

FIGURE 3.

(*Left*) Positions of R2220 and R2320 in FVIII C2 with Spikes 1-4 highlighted in blue. (*Right*) 90°-rotated (towards the right from the left panel) cross section view of FVIII C2 (cyan wire presentation and black half-transparent surface; Spikes highlighted in blue) with a bound PS headgroup interacting with R2320 of the characteristic soft 'funnel' PS pocket. Snapshot was taken from trajectory #5 at $t = 21$ ns.

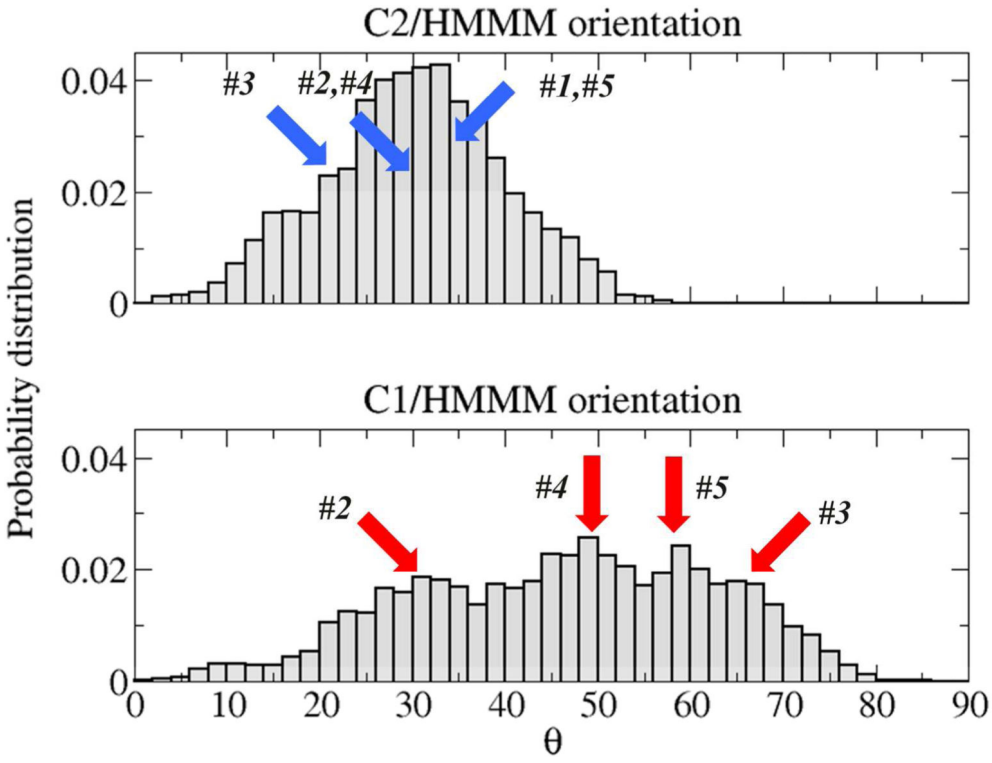

FIGURE 4.

Distribution of the domain tilt angle, θ, of FVIII C2 (top) and FVIII C1 (bottom) for productive membrane-binding trajectories (#1-#5 for FVIII C2, and #2-#5 for FVIII C1). Domain tilt angles corresponding to the final configurations are indicated by arrows.

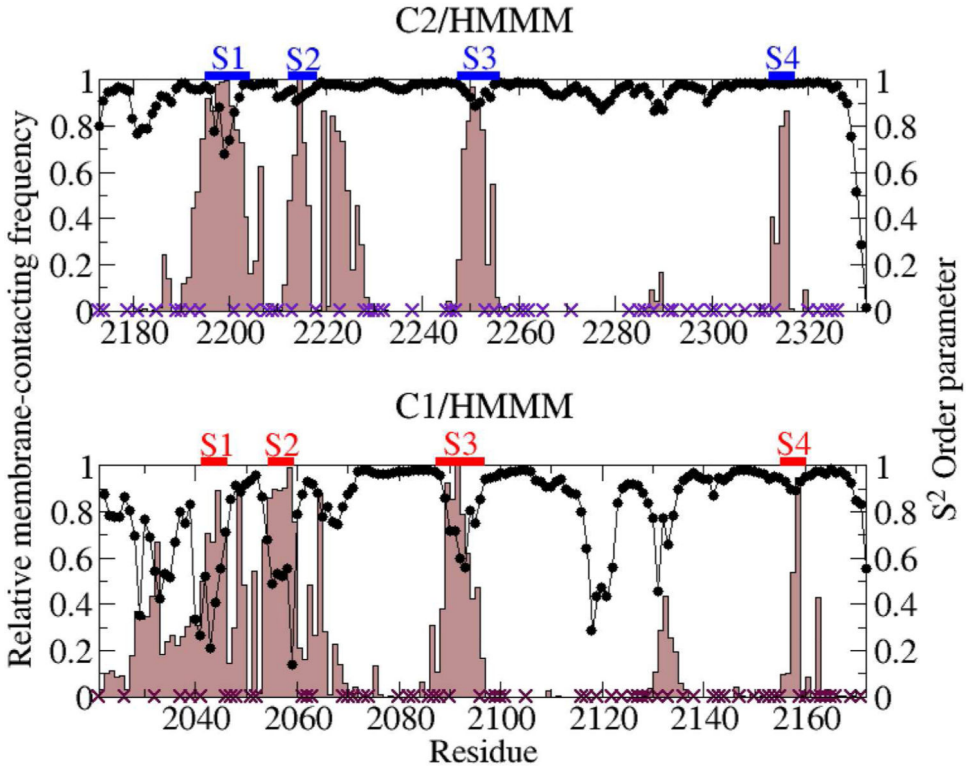

FIGURE 5.

Backbone ($C_i - N_i$ vector) S^2 order parameters (black circles) and membrane contact frequencies (brown shaded bars) for FVIII C2 (top) and FVIII C1 (bottom) in their membrane-bound states. The positions of the spikes (S1-S4) are indicated above the panel (blue bars for FVIII C2 and red bars for FVIII C1). Hemophilic missense mutations are marked with crosses on the baselines.

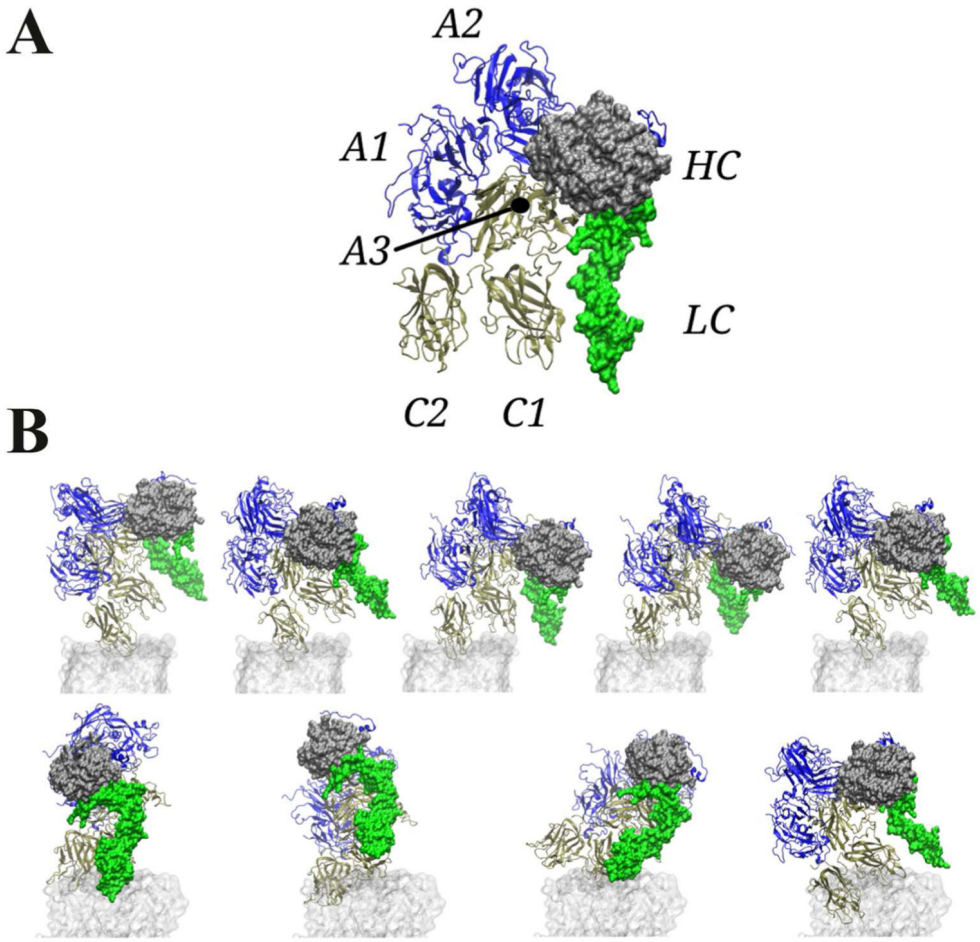

FIGURE 6.

(**A**) Our constructed model of the FVIIIa:FIXa (tenase) complex. B-domain deleted FVIIIa (domains A1-A2-A3-C1-C2) is shown in cartoon representation (A1-A2 in blue, A3-C1-C2 in tan). FIXa is drawn using a surface representation (HC: heavy chain in gray, LC: light chain in green). (**B**) The tenase complex model structurally aligned with and overlaid on the converged membrane-bound individual C2-like domains (*top*: C2/HMMM trajectories #1-#5 from left to right, *bottom*: C1/HMMM trajectories #2-#5 from left to right).

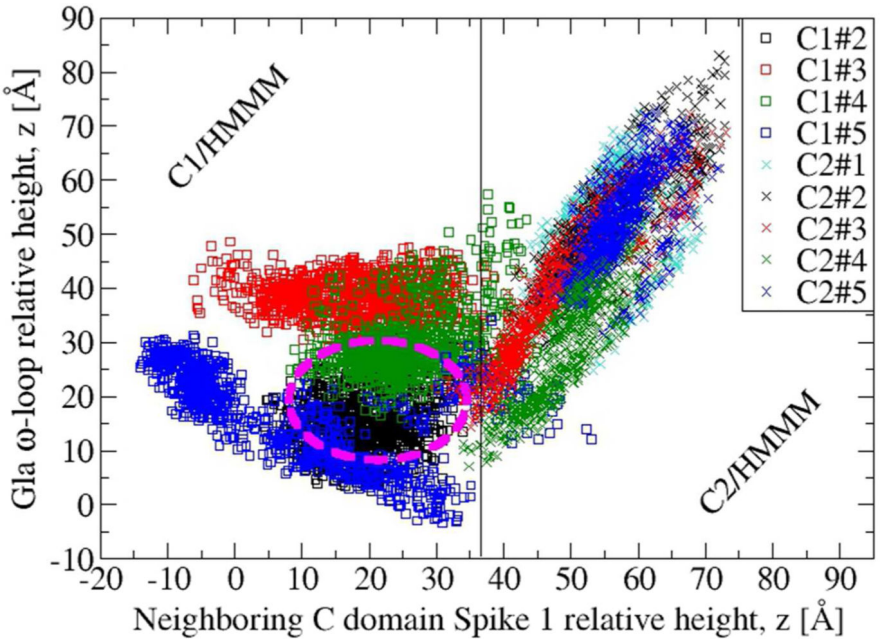

FIGURE 7.

Scatter plot of relative heights, *z*, of the FIX Gla ω-loop (L6, α-carbon) as well as Spike 1 from FVIII C2 (G2044, α-carbon) or FVIII C1 (M2199, α-carbon) calculated based on structural alignment of the putative tenase complex model onto simulation trajectory frames from C2/HMMM (squares) or C1/HMMM (crosses). The abscissa shows the relative height of the neighboring C domain Spike 1, i.e. FVIII C1 Spike 1 for C2/HMMM trajectories, and vice versa. The ordinate shows in all cases the relative height of the FIX Gla-domain ω-loop. The dashed ellipse (magenta) indicates relative heights corresponding to reasonable modes of interaction of the membrane-anchoring domains (roughly z = 15-25 Å). The vertical line approximately separates simulations C1/HMMM (*mostly left*) and C2/HMMM (*mostly right*). Individual trajectories are consistently color-coded (#1 in cyan, #2 in black, #3 in red, #4 in green, and #5 in blue).

TABLE 1

Overview and component count of the simulated systems.

System	Lipid type	Area / lipid [A^2][1]	No. of trajectories	Spontaneous binding observed in	Simulation time per trajectory [ns]	No. of water molecules	No. of atoms
C1/HMMM	PS	88.5	5	All except #1	50-55	~7,800	~37,000
C2/HMMM	PS	85.0	5	All	~37	~7,700	~37,000
C2/Soln	-	-	1	-	50	~4,600	~16,400

[1] Before the insertion of the protein.